

# Robust Moving Target Defence Against False Data Injection Attacks in Power Grids

Wangkun Xu<sup>1</sup>, Imad M. Jaimoukha<sup>1</sup>, and Fei Teng<sup>1</sup>, *Senior Member, IEEE*

**Abstract**—Recently, moving target defence (MTD) has been proposed to thwart the false data injection (FDI) attacks in power system state estimation by proactively triggering the distributed flexible AC transmission system (D-FACTS) devices. One of the key challenges for MTD in power grid is to design its real-time implementation with performance guarantees against unknown attacks. Converting from the noiseless assumptions in the literature, this paper investigates the MTD design problem in a noisy environment and proposes, for the first time, the concept of robust MTD to guarantee the worst-case detection rate against all unknown attacks. We theoretically prove that, for any given MTD strategy, the minimal principal angle between the Jacobian subspaces corresponds to the worst-case performance against all potential attacks. Based on this finding, robust MTD algorithms are formulated for the systems with both complete and incomplete configurations. Extensive simulations using standard IEEE benchmark systems demonstrate the improved average and worst-case performances of the proposed robust MTD against state-of-the-art results.

**Index Terms**—Cyber physical power system, false data injection attacks, moving target defence, principal angles and vectors.

## I. INTRODUCTION

### A. Background

THE EMERGING implementation of information techniques has reformed the power grid into a complex cyber-physical power system (CPPS), where the two-way real-time communication among multiple parties raises new risks in the grid [1]. Musleh *et al.* [2] reviewed seven recent cyber attacks in energy industry and spotted the related vulnerabilities in both physical and cyber layers. Recently, false data injection (FDI) attacks have been developed against power system state estimation (SE) by intruding through the Modbus/TCP protocol without being noticed by the bad data detector (BDD) at the control centre [3]–[6]. As the accurate state estimation is crucial for energy management system (EMS) activities, such as power system dispatch, contingency analysis, and fault diagnosis, states falsified by the FDI attacks can result in erroneous control action, causing economic losses, system instability, and safety violation [7]–[9].

As the power system operates quasi-statically, the intruders have sufficient time to learn the system parameters and preparing the FDI attacks [10]–[12]. As a result, it is crucial to invalidate the attacker’s knowledge by proactively changing the system configuration. Moving target defence (MTD), which is firstly conceptualized for the information technology security,

utilizes this proactive defence idea [13]. With the distributed flexible AC transmission system (D-FACTS) devices, the control centre can alter the reactances of the transmission lines to physically change the system parameters that are unknown to the attackers.

### B. Related Work

Initially, researches on MTD involve using random placement and reactance perturbations to expose FDI attacks [14]–[16]. However, it has been shown that the so-called ‘naive’ applications cannot guarantee an effective detection on stealthy FDI attacks. Therefore, [17] and [18] demonstrate that the MTD effectiveness is dependent on the rank of the composite pre- and post- MTD measurement matrices. Furthermore, Liu, *et al.* [19] and Zhang *et al.* [20] investigate the D-FACTS devices placement in the planning stage to maximize the effectiveness while minimising the investment budget. The authors in [21] analyze the MTD effectiveness using the metric of minimal principal angle and numerically show the relationship between the angle and the average detection rate, which can be used to design the MTD. Liu, *et al.* [22] extends the MTD strategy in [17] with sensor protections and Tian, *et al.* [23] applies MTD to detect Stuxnet-like attack. Moreover, Higgins *et al.* [24] suggests to perturb the reactance through Gaussian watermarking to prevent the attacker from inferring the new system parameters. However, majority of the above literature studies the effectiveness of MTD under DC and noiseless assumptions. As demonstrated by [25], the MTD detection rate is limited by the ratio between the attack strength and the noise level. As a result, there is no guarantee on the detection performance of existing MTD strategies against the unseen attacks in a noisy environment.

### C. Contributions

With the attackers becoming more resourceful and intelligent, it becomes harder to anticipate the attackers’ strategy. Therefore, it is critical for the system operator to determine and guarantee the lowest detection rate of MTD against all unknown attacks. In this context, this paper introduces the concept of *robust MTD*, which aims to guarantee the worst-case MTD effectiveness against a given level of attack strength under noisy environment. The main contributions of this paper are summarized as follows.

- This paper, for the first time, proposes the concept of robust MTD in a noisy environment. We theoretically proves that, for any given grid topology and MTD strategy, the minimal principal angle between the pre-

<sup>1</sup>The authors are with the Department of Electrical and Electronic Engineering, Imperial College London, London, SW7 2AZ, U.K. Corresponding author: Dr Fei Teng (f.teng@imperial.ac.uk).

and post-MTD Jacobian subspaces is directly linked with the worst-case performance against all potential attacks, which can be used as a new metric to represent the MTD effectiveness.

- A novel MTD design algorithm is formulated to improve the worst-case detection rate by maximizing the minimal principal angle under the complete grid configuration. We then demonstrate that the worst-case detection rate of the grid with incomplete configuration cannot be improved. Therefore, an iterative algorithm is formulated to maximize the minimal nonzero principal angle while limits the chance of attacking on the subspace that cannot be detected.
- Numerical simulations on IEEE case-6, 14, and 57 systems demonstrate the improved detection performance of the robust MTD algorithms against the worst-case, random, and single-state attacks, under both simplified and full AC models.

The rest of the paper is organized as follows. The preliminaries are summarised in Section II; Analysis on MTD effectiveness is presented in Section III; Problem formulation and the proposed robust algorithms are presented in Section IV; Case studies are given in Section V with conclusions in Section VI.

## II. PRELIMINARIES

### A. Notations

In this paper, vectors and matrices are represented by bold lowercase and uppercase letters, respectively. The  $p$ -norm for  $\mathbf{a}$  is written as  $\|\mathbf{a}\|_p$ . The column space of  $\mathbf{A}$  is  $\mathcal{A} = \text{Col}(\mathbf{A})$ .  $\mathbf{P}_\mathbf{A} = \mathbf{A}(\mathbf{A}^T\mathbf{A})^{-1}\mathbf{A}^T$  represents the orthogonal projector to  $\text{Col}(\mathbf{A})$  while  $\mathbf{S}_\mathbf{A} = \mathbf{I} - \mathbf{P}_\mathbf{A}$  represents the orthogonal projector to  $\text{Kel}(\mathbf{A}^T)$ . The set of singular values is  $\sigma(\mathbf{A}) = \{\sigma_1(\mathbf{A}), \sigma_2(\mathbf{A}), \dots, \sigma_{\min\{m,n\}}(\mathbf{A})\}$ . The spectral norm is  $\|\mathbf{A}\| = \max_i \sigma_i(\mathbf{A})$  and the Frobenius norm is  $\|\cdot\|_F$ . We use  $(\cdot)'$  symbol to indicate the quantities after MTD and  $(\cdot)_a$  to indicate the quantities after the attack. Matrix operator  $\circ$  represents Hadamard product. Other symbols and operators are defined in the paper whenever proper.

### B. System Model and State Estimation

In this paper, the power system is modelled as a graph  $\mathcal{G}(\mathcal{N}, \mathcal{E})$  with  $|\mathcal{N}| = n + 1$  number of buses and  $|\mathcal{E}| = m$  number of branches. For each bus, we denote its complex voltage as  $\boldsymbol{\nu} = \boldsymbol{\nu} \angle \boldsymbol{\theta}$ ; and for each branch, we denote the admittance as  $\mathbf{y} = \mathbf{g} + j\mathbf{b}$ . The power system can be modelled by the nonlinear equations  $\mathbf{z} = \mathbf{h}(\boldsymbol{\nu}) + \mathbf{e}$  where  $\mathbf{z} \in \mathbb{R}^p$  is the sensor measurement;  $\mathbf{h}(\cdot) \in \mathbb{R}^p$  is the power balancing equation;  $\boldsymbol{\nu} \in \mathbb{R}^{2(n+1)}$  is the system state composing of voltage magnitude and phase angle. The measurement noise vector  $\mathbf{e} \in \mathcal{N}(\mathbf{0}, \mathbf{R})$  follows independent Gaussian distribution with diagonal covariance matrix  $\mathbf{R} = \text{diag}([\sigma_1^2, \sigma_2^2, \dots, \sigma_p^2])$ . In detail,  $\mathbf{h}(\cdot)$  is considered as [7]:

$$P_i = v_i \sum_{j=1}^n v_j (g_{ij} \cos \theta_{ij} + b_{ij} \sin \theta_{ij}) \quad (1a)$$

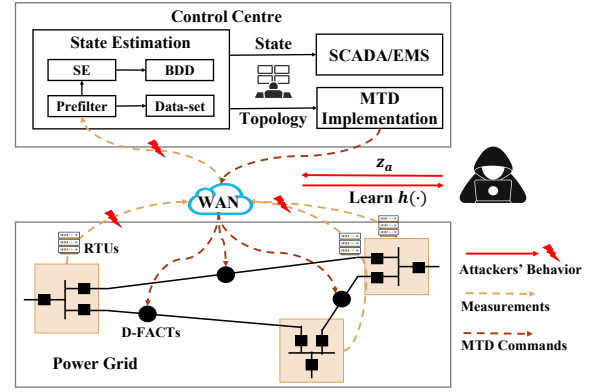


Figure 1: EMS with injection attacks and MTD in CPPS.

$$Q_i = v_i \sum_{j=1}^n v_j (g_{ij} \sin \theta_{ij} - b_{ij} \cos \theta_{ij}) \quad (1b)$$

$$P_{k:i \rightarrow j} = v_i v_j (g_{ij} \cos \theta_{ij} + b_{ij} \sin \theta_{ij}) - g_{ij} v_i^2 \quad (1c)$$

$$Q_{k:i \rightarrow j} = v_i v_j (g_{ij} \sin \theta_{ij} - b_{ij} \cos \theta_{ij}) + b_{ij} v_i^2 \quad (1d)$$

where  $P_i$  and  $Q_i$  are the active and reactive power injections at bus  $i$ ; and  $P_{k:i \rightarrow j}$  and  $Q_{k:i \rightarrow j}$  are the  $k$ -th active and reactive power flows from bus  $i$  to  $j$ ;  $\theta_{ij} = \theta_i - \theta_j$  is the phase angle difference between bus  $i$  and  $j$ ;

As shown in Fig. 1, the control centre is equipped with state estimation (SE) serving as a bridge between remote terminal units (RTUs) and energy management system (EMS) [7]. Given the measurements, the AC-SE is solved by the following weighted least-square problem using iterative algorithm, such as Gauss-Newton method [26]:

$$\min_{\hat{\boldsymbol{\nu}}} J(\hat{\boldsymbol{\nu}}) = (\mathbf{z} - \mathbf{h}(\hat{\boldsymbol{\nu}}))^T \cdot \mathbf{R}^{-1} \cdot (\mathbf{z} - \mathbf{h}(\hat{\boldsymbol{\nu}})) \quad (2)$$

where  $\hat{\boldsymbol{\nu}}$  is the estimated state. Furthermore, the bad data detection (BDD) at the control centre detects any measurement error that violates a Gaussian prior. Given  $\hat{\boldsymbol{\nu}}$ , the residual vector is calculated as  $\mathbf{r} = \mathbf{z} - \mathbf{h}(\hat{\boldsymbol{\nu}})$  and the residual is represented as  $\gamma(\mathbf{z}) = \|\mathbf{R}^{-\frac{1}{2}} \mathbf{r}\|_2^2$ . Let  $\mathbf{e}$  be the random variable; then  $\gamma$  approximately follows  $\chi^2$  distribution with degree of freedom (DoF)  $p - 2n$  [26]. The threshold  $\tau_\chi(\alpha)$  of the  $\chi^2$  detector can be defined probabilistically based on the desired False Positive Rate (FPR)  $\alpha \in (0, 1)$  by the system operator [26]:

$$\int_{\tau_\chi(\alpha)}^{\infty} g(u) du = \alpha \quad (3)$$

where  $g(u)$  is the p.d.f of the  $\chi^2$  distribution and  $\alpha$  is usually set as 1%-5%.

### C. Attack Assumptions

With the emerging implementation of information and communication techniques, standard protocols, such as Modbus can be vulnerable to FDI attacks. It has been shown that an FDI attack  $\mathbf{z}_a = \mathbf{z} + \mathbf{a}$  can pass the BDD if  $\mathbf{a} = \mathbf{h}(\boldsymbol{\nu} + \mathbf{c}) - \mathbf{h}(\boldsymbol{\nu})$  where  $\mathbf{c}$  is the attack vector on the state vector. In this case, the contaminated measurement becomes  $\mathbf{z}_a = \mathbf{h}(\boldsymbol{\nu} + \mathbf{c}) + \mathbf{e}$  whose residual follows the same  $\chi^2$

distribution as the legit measurement  $z$ . It also implies that, an attacker against AC state estimation has to know the exact formulation of  $\mathbf{h}(\cdot)$  and the value of the state  $\nu$  to avoid being detected. To successfully launch such attack, we assume the attacker's abilities as follows:

**Assumption 1:** The attackers can access all the measurements and are aware of the admittance and topology of the grid to build  $\mathbf{h}(\cdot)$ . The exfiltration can be achieved by data-driven algorithms [10]–[12], [27]. However, the duration of data collection is much longer than a single state estimation time, implying that the attacker cannot immediately know the exact value of reactance changes [21]. Meanwhile, the attackers are also aware of the exact state or state estimation from the previous measurements [4], [5].

**Assumption 2:** The attackers can modify or replace all the eavesdropped measurements to achieve the attack purpose. However, as large instant measurement change may violate the temporal trends of the grid measurements and be detected [21], [22], [28], [29], the attack strength  $\|\mathbf{a}\|_2$  is assumed to be limited.

Assumption 1-2 require the attacker's efforts to gain sufficient knowledge on the grid topology and operational conditions which may not be easy in practice. However, we assume a strong attack ability and study the defence algorithm against the most general and unpredictable FDI attacks.

#### D. Moving Target Defence

By using the D-FACTS devices, the system operator can proactively change the reactances to keep invalidating the attacker's knowledge on  $\mathbf{h}(\cdot)$ :

$$\mathbf{h}_x(\cdot) \xrightarrow{\text{D-FACTS}} \mathbf{h}_{x'}(\cdot)$$

where  $x' = x + \Delta x$  is the reactance after triggering the D-FACTS devices. As illustrated by Fig. 1, the channels of D-FACTS devices are encrypted and MTD is implemented with period shorter than the reconnaissance time of the attacker (see Assumption 1). In addition, the reactance changed by the D-FACTS devices are limited physically:

$$-\tau x_i \leq \Delta x_i \leq \tau x_i, \quad i \in \mathcal{E}_D \quad (4a)$$

$$\Delta x_i = 0, \quad i \in \mathcal{E} \setminus \mathcal{E}_D \quad (4b)$$

where  $\tau$  represents the maximum perturbation ratio of D-FACTS devices. Typical values of  $\tau$  are reported as 20%–50% in literature [17]–[19], [21];  $\mathcal{E}_D$  represents the branch set equipped with the D-FACTS devices. After implementing MTD, the residual vector becomes  $\mathbf{r}'_a = \mathbf{h}'(x) + \mathbf{h}(x + c) - \mathbf{h}(x) + e$  which may not follow the  $\chi^2$  distribution of the legit measurement any more and hence trigger the bad data detector.

#### E. Model Simplification for MTD Design

To design the MTD against FDI attacks, most of the literature relies on either DC or simplified AC power system models [17]–[22], [25] and then verifies the performance on the full AC model. Here we adopt the simplified AC model based on the linearized measurement equation. Compared with

the DC model, the simplified AC model can reflect on different state values with the branch resistance also considered.

In detail, the first-order Taylor expansion can be established around a stationary state  $\nu_0$ :

$$z = \mathbf{h}(\nu_0) + \mathbf{J}_{\nu_0}(\nu - \nu_0) + e \quad (5)$$

where the Jacobian matrix of  $\mathbf{h}(\cdot)$  is found with respect to  $\nu_0$  as  $\mathbf{J}_{\nu_0} = \left[ \frac{\partial \mathbf{h}_k}{\partial \nu_i} \Big|_{\nu=\nu_0} \right]_{i,k}$ . The state  $\nu_0$  can be simulated from security constrained AC-OPF [7] around the estimated active and reactive loads before the real-time operation. Alternatively, the states estimated from the previous measurements or a flat state [22], [30] can also be used. Following the recent literature on MTD [17], [19], [22], we consider the FDI attacks on the voltage phase angle and derive the defence strategies according to the power flow measurements at each branch. Therefore, the Jacobian matrix is considered as:

$$\left[ \frac{\partial \mathbf{P}_{k:i \rightarrow j}}{\partial \theta_i} \Big|_{\theta=\theta_0} \right]_k = -\mathbf{V} \cdot \mathbf{G} \cdot \mathbf{A}_r^{\sin} + \mathbf{V} \cdot \mathbf{B} \cdot \mathbf{A}_r^{\cos} \quad (6)$$

where  $\mathbf{V} = \text{diag}((\mathbf{C}_f \mathbf{v}) \circ (\mathbf{C}_t \mathbf{v}))$ ;  $\mathbf{G} = \text{diag}(g)$ ;  $\mathbf{B} = \text{diag}(b)$ ;  $\mathbf{A}_r^{\sin} = \text{diag}(\sin \mathbf{A} \theta_0) \mathbf{A}_r$ ; and  $\mathbf{A}_r^{\cos} = \text{diag}(\cos \mathbf{A} \theta_0) \mathbf{A}_r$ . Moreover,  $\mathbf{C}_f$  and  $\mathbf{C}_t$  are the 'from' and 'to' -side incidence matrices;  $\mathbf{A}_r$  is the reduced incidence matrix by removing the column representing the reference bus from incidence matrix  $\mathbf{A}$ . To simplify the notation, we omit the subscript  $\theta_0$  in the following discussion.

According to Assumption 2, as the attack strength is limited, the attack vector can also be linearized around  $\theta_0$  as [22]:

$$\mathbf{a} = \mathbf{h}(\theta_0 + c) - \mathbf{h}(\theta_0) = \mathbf{J}c \quad (7)$$

We design the MTD algorithm based on the simplified AC model (5)-(7) using active power flow measurements. The designed MTD will be then applied on the original AC model (1)-(2) to verify the performance.

### III. ANALYSIS ON MTD EFFECTIVENESS

In this section, we firstly extend the concept of complete MTD in the literature from DC model to simplified AC model. We then define the MTD effectiveness in a probabilistic way and illustrate the need for new metric on effective MTD design in a noisy environment.

#### A. Complete MTD

Let  $\mathbf{H}$  and  $\mathbf{H}'$  be the DC measurement matrices. Under the noiseless condition, the *complete MTD* can be designed to detect any FDI attack by keeping the composite matrix  $[\mathbf{H}, \mathbf{H}']$  full column rank [17]–[20]. If the full rank condition cannot be achieved due to the sparse grid topology (e.g.  $m < 2n$ ) or limited D-FACTS devices, a *max-rank incomplete MTD* can be designed to minimize the attack space. As the rank of the composite matrix is maximized in both complete and incomplete conditions, we refer the MTD strategies in [17]–[20] as *max-rank MTD*.

To help better define the problem, we extend the concept of complete and incomplete MTDs from the DC model to the simplified AC models in the following proposition:

**Proposition 1.** *The power system modelled by (5) is with complete configuration against the FDI attack modelled by (7) only if  $m \geq 2n$ .*

*Proof.* Please refer to Appendix A  $\square$

As stated by Proposition 1, to have complete configuration  $\text{rank}([\mathbf{J}_N, \mathbf{J}'_N]) = 2n$ , the number of branches should be at least one time larger than the number of buses. In addition, the max-rank incomplete MTD with  $\text{rank}([\mathbf{J}_N, \mathbf{J}'_N]) = m$  can be designed for the grid with incomplete configuration. In the following discussions, we refer the grid that can achieve complete MTD under certain topology and D-FACTS deployment as *complete configuration*, otherwise as *incomplete configuration*.

### B. $\beta$ -Effective MTD

Following the equation (5), denote  $\mathbf{z} \triangleq \mathbf{z} - \mathbf{h}(\boldsymbol{\theta}_0)$  and  $\boldsymbol{\theta} \triangleq \boldsymbol{\theta} - \boldsymbol{\theta}_0$ . For the new system equation  $\mathbf{z} = \mathbf{J}\boldsymbol{\theta} + \mathbf{e}$ , the residual vector of the  $\chi^2$  detector can be written as  $\mathbf{r} = \mathbf{S}(\mathbf{J}\boldsymbol{\theta} + \mathbf{e}) = \mathbf{S}\mathbf{e}$  where  $\mathbf{S} = \mathbf{I} - \mathbf{J}(\mathbf{J}^T \mathbf{R}^{-1} \mathbf{J})^{-1} \mathbf{J}^T \mathbf{R}^{-1}$  is the weighted orthogonal projector on  $\text{Ker}(\mathbf{J}^T)$ . The residual  $\gamma = \|\mathbf{R}^{-\frac{1}{2}} \mathbf{S}\mathbf{e}\|^2$  follows the  $\chi^2$  distribution with DoF  $m - n$ . Referring to the simplified attack model (7), the residual vector after MTD under attack can be written as  $\mathbf{r}'_a = \mathbf{S}'(\mathbf{J}\mathbf{c} + \mathbf{e})$  where  $\mathbf{S}' = \mathbf{I} - \mathbf{J}'(\mathbf{J}'^T \mathbf{R}^{-1} \mathbf{J}')^{-1} \mathbf{J}'^T \mathbf{R}^{-1}$ . As  $\mathbf{a}$  is usually not in  $\mathcal{J}'$  and  $\mathbf{r}'_a$  is biased from zero, the residual  $\gamma'_a = \|\mathbf{R}^{-\frac{1}{2}} \mathbf{S}'(\mathbf{J}\mathbf{c} + \mathbf{e})\|^2$  follows the non-central  $\chi^2$  distribution, i.e.  $\gamma'_a \sim \chi^2_{m-n}(\lambda)$  with non-centrality parameter  $\lambda = \|\mathbf{R}^{-\frac{1}{2}} \mathbf{S}' \mathbf{J} \mathbf{c}\|_2^2$  [31]. Meanwhile, the mean and variance of the distribution are given as  $\mathbf{E}(\gamma'_a) = m - n + \lambda$  and  $\mathbf{Var}(\gamma'_a) = 2(m - n + 2\lambda)$ , respectively. It is clear that when a noisy environment is considered, the deterministic criteria can not be used any more to describe the effectiveness of MTD. A probabilistic criteria is hence defined below. For clear presentation, the matrices are normalized with respect to the measurement noises (see Appendix B).

Followed by (3), for any given attack vector  $\mathbf{a}$ , we define an MTD as  $\beta$ -effective ( $\beta$ -MTD in short) if the following inequality is satisfied:

$$f(\lambda) = \int_{\tau_{\chi}(\alpha)}^{\infty} g_{\lambda}(u) du \geq \beta \quad (8)$$

where  $g_{\lambda}(u)$  is the p.d.f. of non-central  $\chi^2$  distribution. When  $\lambda$  increases from 0, the detection probability on  $\mathbf{a}$  also increases as the mean and variance increase [32]. Therefore, for a given  $\beta$ , there exists a minimum  $\lambda$  such that (8) is satisfied, which is defined as critical  $\lambda$  and denoted as  $\lambda_c(\beta)$ .

Consequently, the rank conditions in [17]–[20], [22] cannot guarantee the detection performance as they are not directly linked with the increase of  $\lambda$  to have  $\beta$ -MTD. Fig. 2 illustrates the c.d.f. of  $\gamma'$  on a random FDI attack using max-rank MTDs in a case-14 system. Without using MTD, the detection rate is 5% which is consistent with the FPR. To have high detection rate, e.g.  $\beta = 95\%$ , it is desirable to sufficiently shift the distribution as shown by the blue curve. For the max-rank MTDs that satisfy max-rank condition, they can shift the c.d.f. positively, but there is no guarantee on how much of such shift can be achieved and whether it leads to the desired detection

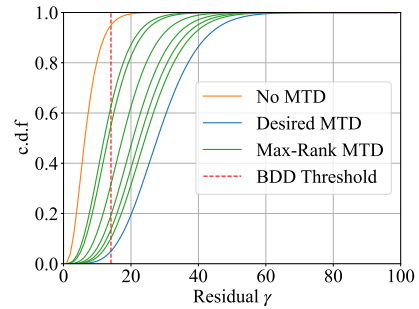


Figure 2: Illustration of attack detection probability on IEEE case-14 system based on simplified AC model (5)-(7). The more positively the c.d.f. is shifted, the higher averaged detection rate can be achieved.

rates. This finding clearly calls for new criterion to guide the design of MTD in a noisy environment.

Moreover, as numerically shown by [25], not all attacks can be detected by the MTD with high detection rate. Therefore, we theoretically introduce the following necessary condition to have  $\beta$ -MTD which can be seen as the limitation of MTD against FDI attacks with small attack strength.

**Proposition 2.** *An MTD is  $\beta$ -effective only if  $\|\mathbf{a}_N\|_2 \geq \sqrt{\lambda_c(\beta)}$ .*

*Proof.* Please refer to Appendix C.  $\square$

Proposition 2 can be further analyzed on  $\mathbf{a}$  to have  $\|\mathbf{a}\|_2 \geq \sigma_{\min} \sqrt{\lambda_c(\beta)}$  with  $\sigma_{\min} = \min_i \{\sigma_1, \sigma_2, \dots, \sigma_m\}$ . This implies that  $\beta$ -MTD can be achieved only if the ratio between attack strength and measurement noise is higher than a certain value, which verifies the numerical results in [25].

### C. Max MTD

While Proposition 2 establishes the theoretic limit on the detection probability for any given attack strength, in practise, the constraints on the D-FACTS devices (4a)-(4b) will further restrict such limit. In this context, the maximum detection rate on a known attack vector  $\mathbf{a}_N$ , with the limits of D-FACTS devices considered, can be found by the *max-MTD* algorithm:

$$\begin{aligned} \max_{\Delta \mathbf{x}} \quad & \|\mathbf{S}'_N \mathbf{a}_N\|_2^2 \\ \text{s.t.} \quad & (4a) - (4b) \end{aligned} \quad (9)$$

*max-MTD* can be used to evaluate the MTD effectiveness against any known attack vector. However, it is impossible to design  $\Delta \mathbf{x}$  to achieve certain  $\lambda_c(\beta)$  in advance when  $\mathbf{a}_N$  is not known. Instead, *max-MTD* can be regarded as the performance upper-bound for any MTD strategies with the same placement and perturbation limit.

## IV. ROBUST MTD ALGORITHMS

In this section, we start by establishing the concept of robust MTD and its mathematical formulation. Then the robust MTD algorithms are formulated for the grid with complete and incomplete configurations, respectively.

### A. Definition and Problem Formulation

Instead of considering the average detection rate, this paper defines the robust MTD that can maximise the worst-case detection rate against all possible attacks. Firstly, we define the weakest point for a given MTD design as follows.

**Definition 1.** Given  $\Delta\mathbf{x}$  and the corresponding pair of subspaces  $(\mathcal{J}_N, \mathcal{J}'_N)$ , the weakest point of  $(\mathcal{J}_N, \mathcal{J}'_N)$  is defined as an unitary element  $\mathbf{j}_N^* \in \mathcal{J}_N$  such that  $\lambda(\Delta\mathbf{x}, \mathbf{j}_N^*) \leq \lambda(\Delta\mathbf{x}, \mathbf{j}_N)$  for  $\forall \mathbf{j}_N \in \mathcal{J}_N$ ,  $\|\mathbf{j}_N\|_2 = 1$ . The worst-case detection rate on attack strength  $\|\mathbf{a}_N\|_2 = |a| \neq 0$  is defined as  $f(\lambda_{\min})$  with  $\lambda_{\min} = \lambda(\Delta\mathbf{x}, \mathbf{a}_N^*)$ .

According to the Definition 1, the weakest point in  $(\mathcal{J}_N, \mathcal{J}'_N)$  satisfies  $|a|\|\mathbf{S}'_N \mathbf{j}_N^*\|_2 \leq |a|\|\mathbf{S}'_N \mathbf{j}_N\|_2$ ,  $\forall \mathbf{j}_N \in \mathcal{J}_N$ ,  $\|\mathbf{j}_N\|_2 = 1$ ,  $a \neq 0$ . Let  $\mathbf{a}_N^* = \mathbf{a}_N \mathbf{j}_N^*$  and  $\mathbf{a}_N = \mathbf{a}_N \mathbf{j}_N$ , the detection rate on  $\mathbf{a}_N^*$  is the lowest among all attacks with the same strength as  $\|\mathbf{S}'_N \mathbf{a}_N^*\|_2 \leq \|\mathbf{S}'_N \mathbf{a}_N\|_2$ ,  $\forall \mathbf{a}_N \in \mathcal{J}_N$ ,  $\|\mathbf{a}_N\|_2 = |a| \neq 0$ . Note that the weakest point may not be unique, but all of them are with the same worst-case detection rate.

Based on the definition of MTD weakest point, the following robust max-min optimization problem can be formulated:

$$\begin{aligned} \max_{\Delta\mathbf{x}} \min_{\|\mathbf{a}_N\|_2=1, \mathbf{a}_N \in \mathcal{J}_N} & \|\mathbf{S}'_N \mathbf{a}_N\|_2^2 \\ \text{s.t.} & \quad (4a) - (4b) \end{aligned} \quad (10)$$

The inner problem  $\min_{\|\mathbf{a}_N\|_2=1, \mathbf{a}_N \in \mathcal{J}_N} \|\mathbf{S}'_N \mathbf{a}_N\|_2^2$  is the mathematical formulation of the weakest point in Definition 1 which is maximized over the outer programming. From a game theorem point of view, we can present this setting as an intelligent attacker aims to develop an FDI attack with the highest probability to bypass BDD and the system operator tries to improve his/her defence strategy against this intelligent attacker. In the following sections, we will show that the two-stage problem (10) can be reduced into a single-stage minimization problem by analytically representing the weakest point using the principal angles between  $\mathcal{J}_N$  and  $\mathcal{J}'_N$ .

### B. Robust MTD for the Grid with Complete Configuration

Similar to the one-dimensional case where the angle between two unitary vectors  $\mathbf{u}$  and  $\mathbf{v}$  is defined as  $\cos \theta = \mathbf{v}^T \mathbf{u}$ , the minimal angle between  $\mathcal{J}_N, \mathcal{J}'_N \subseteq \mathbb{R}^p$  is defined as  $0 \leq \theta_1 \leq \pi/2$  [33]:

$$\cos \theta_1 = \max_{\substack{\mathbf{u} \in \mathcal{J}_N, \mathbf{v} \in \mathcal{J}'_N \\ \|\mathbf{u}\|_2 = \|\mathbf{v}\|_2 = 1}} \mathbf{u}^T \mathbf{v} = \mathbf{u}_1^T \mathbf{v}_1 \quad (11)$$

Apart from  $\theta_1$ , a sequence of angles can be defined iteratively by finding the orthonormal basis of  $\mathcal{J}_N$  and  $\mathcal{J}'_N$  such that for  $i = 2, \dots, n$  [33]:

$$\cos \theta_i = \max_{\substack{\mathbf{u} \in \mathcal{J}_N, \mathbf{v} \in \mathcal{J}'_N \\ \|\mathbf{u}\|_2 = \|\mathbf{v}\|_2 = 1}} \mathbf{u}^T \mathbf{v} = \mathbf{u}_i^T \mathbf{v}_i \quad (12)$$

where  $\mathcal{J}_{N,i} = \mathbf{u}_{i-1}^\perp \cap \mathcal{J}_{N,i-1}$  and  $\mathcal{J}'_{N,i} = \mathbf{v}_{i-1}^\perp \cap \mathcal{J}'_{N,i-1}$ .

From (11)-(12), a sequence of angles  $\Theta = \{\theta_1, \theta_2, \dots, \theta_n\}$  is defined as the principal angles between  $\mathcal{J}_N$  and  $\mathcal{J}'_N$ . The sequence of  $\theta_i$  can be separated into three parts. Let  $\Theta_1 = \{\theta_i | \theta_i = 0\}$ ,  $\Theta_2 = \{\theta_i | 0 < \theta_i < \pi/2\}$ , and

$\Theta_3 = \{\theta_i | \theta_i = \pi/2\}$  with cardinality equals to  $k$ ,  $r$ , and  $l$  respectively, and  $n = k + r + l$ . The corresponding vectors  $\mathbf{U} = \{\mathbf{u}_1, \mathbf{u}_2, \dots, \mathbf{u}_n\}$  and  $\mathbf{V} = \{\mathbf{v}_1, \mathbf{v}_2, \dots, \mathbf{v}_n\}$  are called as principal vectors which are the orthonormal basis of  $\mathcal{J}_N$  and  $\mathcal{J}'_N$ , respectively. Similarly,  $\mathbf{U}$  and  $\mathbf{V}$  can also be separated into  $\mathbf{U}_1, \mathbf{V}_1, \dots$ . Specifically,  $\mathbf{U}_1 = \mathbf{V}_1 = \mathcal{J}'_N \cap \mathcal{J}_N$  represents the intersection subspace of dimension  $k$  and  $l$  is the dimension of orthogonality. Moreover, it is proved that there always exist semi-orthogonal matrices  $\mathbf{U}$  and  $\mathbf{V}$  for any  $\mathcal{J}_N$  and  $\mathcal{J}'_N$  such that the bi-orthogonality is satisfied [34]:

$$\mathbf{U}^T \mathbf{V} = \text{diag}([\cos \theta_1, \cos \theta_2, \dots, \cos \theta_n]) = \Gamma \quad (13)$$

Referring to (11), the following proposition specifies that the weakest point with the lowest detection rate of  $(\mathcal{J}_N, \mathcal{J}'_N)$  is the first principal vector  $\mathbf{u}_1$  associated to the minimal principal angle  $\theta_1$ .

**Proposition 3.** Given a pair of  $(\mathcal{J}_N, \mathcal{J}'_N)$ , the minimum non-centrality parameter under attack strength  $\|\mathbf{a}_N\|_2 = |a| \neq 0$  is  $\lambda_{\min} = a^2 \sin^2 \theta_1$ . Meanwhile,  $\lambda_{\min}$  is achieved when attacking on the first principal vector  $\mathbf{u}_1$  of  $\mathcal{J}_N$ .

*Proof.* Please refer to Appendix D.  $\square$

As  $\sin \cdot$  is monotonically increasing in  $[0, \pi/2]$ , Proposition 3 implies that (10) can be equivalently solved by:

$$\begin{aligned} \max_{\Delta\mathbf{x}} & \theta_1 \\ \text{s.t.} & \quad (4a) - (4b) \end{aligned} \quad (14)$$

As the orthogonal projector is uniquely defined [33] and also by (13), rewriting  $\mathbf{P}_N = \mathbf{U}\mathbf{U}^T$  and  $\mathbf{P}'_N = \mathbf{V}\mathbf{V}^T$  gives

$$\mathbf{P}_N \mathbf{P}'_N = \mathbf{U}\mathbf{U}^T \mathbf{V}\mathbf{V}^T = \mathbf{U}\Gamma\mathbf{V}^T \quad (15)$$

Eq.(15) is the truncated singular value decomposition (t-SVD) on  $\mathbf{P}_N \mathbf{P}'_N$  where the diagonal matrix  $\Gamma$  contains the first  $n$  largest singular values of  $\mathbf{P}_N \mathbf{P}'_N$ , and  $\mathbf{U}$  and  $\mathbf{V}$  are the first (left- and right-hand)  $n$  singular vectors of  $\mathbf{P}_N \mathbf{P}'_N$ . As  $\sigma(\mathbf{P}_N \mathbf{P}'_N) = \{\mathbf{1}_k, \cos^2 \theta_{k+i} (i = 1, \dots, r), \mathbf{0}_{k+r+i} (i = 1, \dots, l), \mathbf{0}_{n+i} (i = 1, \dots, m - n)\}$ , this t-SVD is an exact decomposition of  $\mathbf{P}_N \mathbf{P}'_N$ .

Based on the t-SVD, Algorithm 1 is proposed to find the weakest point and the worst-case detection rate. For the grid with complete configuration, the composite matrix can be full column rank so that  $k = 0$ . Line 6 outputs the weakest point  $\mathbf{u}_1$  while line 9 outputs the empty intersection subspace. The worst-case detection rate is calculated according to Proposition 3 in line 7. Practically, once the MTD strategy is determined, the weakest point  $\mathbf{u}_1$  of this strategy can be directly spotted. The system operator can therefore evaluate the worst-case detection rate with respect to a maximum tolerable attack strength  $|a|$ . In addition, when  $\theta_1 = \pi/2$ , Proposition 3 implies that the minimum non-centrality parameter equals to  $a^2$ . As two subspaces  $\mathcal{J}_N$  and  $\mathcal{J}'_N$  are orthogonal if  $\theta_1 = \pi/2$ , Proposition 3 is consistent with the maximum detection probability described in Theorem 1 of [21].

To guarantee the robust detection performance on the weakest point,  $\theta_1$  should be maximized. As  $\cos \theta_1$  is the largest singular value of  $\mathbf{P}_N \mathbf{P}'_N$  by t-SVD, the worst-case detection



---

**Algorithm 1:** Find the Weakest Point(s) and the Worst-Case Detection Rate
 

---

**Input :**  $\mathcal{G}(\mathcal{N}, \mathcal{E})$ ,  $\Delta \mathbf{x}$ , and  $|a|$   
**Output:**  $\mathbf{u}_{k+1}$ ,  $\mathbf{U}_1$ ,  $f_{min}$

- 1 Construct the pre- and post- MTD measurement matrices  $\mathbf{J}_N$  and  $\mathbf{J}'_N$ , respectively;
- 2 Find the orthogonal projectors  $\mathbf{P}_N$  and  $\mathbf{P}'_N$  on  $\mathbf{J}_N$  and  $\mathbf{J}'_N$ . Then do t-SVD (15);
- 3  $rank = \text{rank}([\mathbf{J}_N, \mathbf{J}'_N])$ ; /\* Rank of the composite matrix. \*/
- 4  $k = 2n - rank$ ; /\* The dimension of  $\mathcal{J}'_N \cap \mathcal{J}_N$ . \*/
- 5  $\theta_{k+1} = \Sigma(k+1, k+1)$ ;
- 6  $\mathbf{u}_{k+1} = \mathbf{U}(k+1, k+1)$ ; /\* The weakest point in  $\mathcal{J}_N \setminus (\mathcal{J}'_N \cap \mathcal{J}_N)$ . \*/
- 7  $f_{min} = f(|a|^2 \mathbf{i}^{-2}(\theta_{k+1}))$ ; /\* The worst-case detection rate in  $\mathcal{J}_N \setminus (\mathcal{J}'_N \cap \mathcal{J}_N)$ . \*/
- 8 **if**  $rank = 2n$  **then**
  - /\* Complete MTD configuration. \*/
  - 9  $\mathbf{U}_1 = \emptyset$ ;
- 10 **else**
  - /\* Incomplete MTD configuration. \*/
  - 11  $\mathbf{U}_1 = \mathbf{U}(:, 1:k)$ ;
- 12 **end**

---

rate can be maximized by the *robust MTD* algorithm for the grid with complete configuration as follows:

$$\begin{aligned} \min_{\Delta \mathbf{x}} \quad & \|\mathbf{P}_N \mathbf{P}'_N\| \\ \text{s.t.} \quad & (4a) - (4b) \end{aligned} \quad (16)$$

where the property  $\|\mathbf{P}_N \mathbf{P}'_N\| = \sigma_{\max}(\mathbf{P}_N \mathbf{P}'_N)$  is used and  $\|\mathbf{P}_N \mathbf{P}'_N\| \in [0, 1]$ .

**Remark 1.** The robust MTD algorithm (16) requires sufficient D-FACTS devices placement (as a planning stage problem) to guarantee  $k = 0$ , e.g., using the ‘D-FACTS placement for the complete MTD’ algorithm in [19].

### C. Robust MTD for the Grid with Incomplete Configuration

The robust MTD in (16) is not tractable for power system with incomplete MTD configuration. As  $k \neq 0$ ,  $\theta_1 \equiv 0$  and  $\|\mathbf{P}_N \mathbf{P}'_N\| \equiv 1$  no matter how  $\Delta \mathbf{x}$  is designed. Fig. 3 shows a three-dimensional incomplete-MTD case. The attack  $\mathbf{a}_N$  in green shows a random attack attempt with nonzero  $\lambda$ . However, the weakest point  $\text{Col}(\mathbf{u}_1)$  is not trivial. As the attacker can possibly target on  $\text{Col}(\mathbf{u}_1)$ , the worst-case detection rate equals to FPR constantly. Apart from  $\theta_1$ , every attack in  $\mathbf{U}_1$  is undetectable. The intersection can be regarded as the space of the weakest points, whose dimension is calculated as  $k = 2n - \text{rank}([\mathbf{J}_N, \mathbf{J}'_N]) \neq 0$ . Therefore, the smallest nonzero principal angle (which also corresponds the weakest point in  $\mathcal{J}_N \setminus (\mathcal{J}'_N \cap \mathcal{J}_N)$ ) can be found as  $\theta_{k+1}$  in line 5 of Algorithm 1 with the minimum detection rate calculated in line 7. Meanwhile,  $\mathbf{U}_1$ , corresponding to the subspace that cannot be detected, is calculated in line 11.

To solve the intractable problem for the grid with incomplete configuration, the following design principles are considered which can improve the robust performance of MTD with incomplete configuration:

**Principle 1:** Minimize  $k$ , the dimension of intersection.

**Principle 2:** The attacker shall not easily attack on the intersection subspace  $\mathbf{U}_1$  by chance.

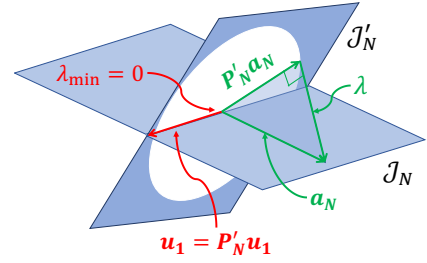


Figure 3: An illustration on the grid with incomplete configuration,  $\mathcal{J}_N, \mathcal{J}'_N \subset \mathbb{R}^3$ .

**Principle 3:** Maximize  $\theta_{k+1}$ , the minimum nonzero principal angle in  $(\mathcal{J}_N, \mathcal{J}'_N)$ .

**Principle 1:** The idea of Principle 1 is to minimize the attack space that can never be detected by MTD so that the probability of detectable FDI attacks increases. Minimizing  $k$  is a planning stage problem as the rank of the composite matrix is almost not related to the perturbation amount of the D-FACTS devices once they are deployed [18]. In this paper, we propose a new D-FACTS device placement algorithm to achieve minimum  $k$ . Compared with the existing work [17]–[19], our algorithm uses the BLOSSOM algorithm [35] to find the maximum cardinality matching [36] of  $\mathcal{G}(\mathcal{N}, \mathcal{E})$ , which can reach all necessary buses with the smallest number of D-FACTS devices. More details are presented in Appendix E.

**Principle 2:** From the robust consideration, the following lemma is derived for the attacks targeting on the weakest point(s) for the grid with incomplete MTD configuration.

**Lemma 1.** Let  $\mathbf{U} = (\mathbf{U}_1, \mathbf{U}_{2,3})$  where  $\mathbf{U}_{2,3}$  is the collection of columns in  $\mathbf{U}_2$  and  $\mathbf{U}_3$ . Let  $\mathbf{a}_N = \mathbf{U}_1 \mathbf{c}_1 + \mathbf{U}_{2,3} \mathbf{c}_{2,3}$  with  $\mathbf{c}_1 \in \mathbb{R}^k$  and  $\mathbf{c}_{2,3} \in \mathbb{R}^{r+l}$ . The detection rate on  $\mathbf{a}_N$  does not depend on the value of  $\mathbf{c}_1$ .

*Proof.* Please refer to Appendix F.  $\square$

Although the attackers cannot immediately know the exact  $\mathbf{x}'$  (Assumption 1), Lemma 1 suggests that the MTD algorithm should be designed such that the attackers cannot easily attack on  $\mathbf{U}_1$  by chance. Specifically, considering the attack targeting on a single state  $i$ , if  $\text{Col}(\mathbf{J}_N(:, i)) \subseteq \mathbf{U}_1$ , the single-state attack on bus  $i$  can bypass the MTD while any attack involving bus  $i$  can be detected ineffectively. To avoid the ineffective MTD on single-state attack, the following constraint is considered:

$$\|\mathbf{P}_N^i \mathbf{P}'_N\| \geq \gamma_i, \quad \forall i \in \mathcal{N}^c \quad (17)$$

where  $\mathbf{P}_N^i = (\mathbf{J}_N(:, i)^T \mathbf{J}_N(:, i))^{-1} \mathbf{J}_N(:, i) \mathbf{J}_N(:, i)^T$  is the orthogonal projector on  $\text{Col}(\mathbf{J}_N(:, i))$ .  $\mathcal{N}^c$  represents the index set of buses that are included by at least a loop<sup>1</sup> of  $\mathcal{G}$ . Since  $\|\mathbf{P}_N^i \mathbf{P}'_N\| \in [0, 1]$  and 1 is achieved when  $\text{Col}(\mathbf{J}_N(:, i)) \subseteq \mathbf{U}_1$ , the threshold  $\gamma_i$  can be set close but not equal to 1.

Notice that the constraint in (17) cannot eliminate the weakest point(s) nor improve the worst-case detection rate on  $\mathbf{U}_1$ , but it can restrict the attacker’s knowledge on the weakest point(s) due to the following reason. Rewriting  $\lambda$  as

<sup>1</sup>As proved by [37], if a bus is not included by any loop, the attacks on this bus cannot be detected regardless of the MTD strategies.

$\lambda = \|(\mathbf{I} - \mathbf{P}'_N) \sum_{i=1}^n \mathbf{J}_N(:, i) \mathbf{c}(i)\|_2^2$ , constraint (17) ensures that  $(\mathbf{I} - \mathbf{P}'_N) \mathbf{J}_N(:, i) \mathbf{c}(i) \neq 0, \forall i \in \mathcal{N}^c$ . To have low MTD detection rate, the attacker has to coordinate the attack strength on at least two bus to have low  $\lambda$  which is only possible if  $\mathbf{x}'$  is known. As long as the attacker cannot easily attack on  $\mathcal{U}_1$ , the probability to have the worst case is low and the MTD strategy is still effective from robust point of view.

**Remark 2.** To fulfill constraint (17), all buses in  $\mathcal{N}^c$  should be incident to at least a branch equipped with D-FACTS devices, which can be achieved by the proposed D-FACTS devices placement algorithm in Appendix E.

**Principle 3:** Although the chance of the worst-case attack is minimized by Principle 1-2, it does not necessarily imply a high detection rate when  $\mathbf{a}_N \notin \mathcal{U}_1$ . Similar to (14), the minimum nonzero principal angle  $\theta_{k+1}$ , which represents the weakest point in subspace  $\mathcal{J}_N \setminus (\mathcal{J}'_N \cap \mathcal{J}_N)$  should be maximized by

$$\begin{aligned} \min_{\Delta \mathbf{x}} \quad & \cos \theta_{k+1} \\ \text{s.t.} \quad & (4a) - (4b), (17) \end{aligned} \quad (18)$$

where  $\cos \theta_{k+1}$  is the  $(k+1)$ th largest singular value.

As far as we know, there is no direct method to solve (18) as finding the singular value at a certain position requires solving the SVD on  $\mathbf{P}_N \mathbf{P}'_N$  and locating the 1th to  $k$ th singular vectors. Therefore, we propose an iterative Algorithm 2 to solve (18). In line 1 of Algorithm 2, a warm start  $\Delta \mathbf{x}^0$  is firstly found by minimizing the Frobenius norm  $\|\cdot\|_F$ , which is shown to be an upper bound to  $\cos \theta_{k+1}$ .

$$\begin{aligned} \min_{\Delta \mathbf{x}} \quad & \|\mathbf{P}_N \mathbf{P}'_N\|_F \\ \text{s.t.} \quad & (4a) - (4b), (17) \end{aligned} \quad (19)$$

For a given warm-start perturbation value  $\Delta \mathbf{x}^0$ , the intersection subspace  $\mathcal{U}_1$  can be located by Algorithm 1. Denoting  $\mathcal{U}_1(\Delta \mathbf{x}^0)$  as  $\mathcal{U}_1^0$ , the t-SVD (15) can be rewritten as

$$\begin{aligned} \mathbf{P}_N \mathbf{P}'_N &= (\mathcal{U}_1^0, \mathcal{U}_{2,3}) \begin{pmatrix} \mathbf{I} & \mathbf{0} \\ \mathbf{0} & \Gamma_{2,3} \end{pmatrix} \begin{pmatrix} \mathbf{V}_1^{0T} \\ \mathbf{V}_{2,3}^T \end{pmatrix} \\ &= \mathcal{U}_1^0 \mathcal{U}_1^{0T} + \mathcal{U}_{2,3} \Gamma_{2,3} \mathcal{V}_{2,3}^T \end{aligned}$$

where  $\mathbf{I}$  is the identity matrix of dimension  $k$ ;  $\Gamma_{2,3} = \text{diag}([\cos(\theta_{k+1}), \dots, \cos(\theta_n)])$  with  $\theta_{k+1} \neq 0$ . Note that  $\mathcal{U}_1^0 = \mathcal{V}_1^0 = \mathcal{J}'_N \cap \mathcal{J}_N$ .

Therefore, the following optimization problem can be formulated to minimize  $\cos \theta_{k+1}$ :

$$\begin{aligned} \min_{\Delta \mathbf{x}} \quad & \|\mathbf{P}_N \mathbf{P}'_N - \mathcal{U}_1^0 \mathcal{U}_1^{0T}\| \\ \text{s.t.} \quad & (4a) - (4b), (17) \end{aligned} \quad (20)$$

Denoting the optimal value of (20) as  $\Delta \mathbf{x}^1$ , a new intersection subspace  $\mathcal{U}_1^1 = \mathcal{U}_1(\Delta \mathbf{x}^1)$  can be located. As  $\Delta \mathbf{x}^1$  is solved with fixed  $\mathcal{U}_1^0$ ,  $\mathcal{U}_1^1$  may not be the same as  $\mathcal{U}_1^0$ . After finding the new intersection subspace from  $\Delta \mathbf{x}^1$ , (20) can be iteratively solved until convergence as shown by line 3-11 in Algorithm 2.

To sum up, Algorithm 2 limits the chance of attacking on  $\mathcal{J}'_N \cap \mathcal{J}_N$  (Principal 1-2) and guarantees the worst-case detection rate in  $\mathcal{J}_N \setminus (\mathcal{J}'_N \cap \mathcal{J}_N)$  (Principal 3 and (19)-(20)) for the grid with incomplete configuration.

---

### Algorithm 2: Robust MTD for the Grid with Incomplete Configuration

---

```

Input :  $\mathcal{G}(\mathcal{N}, \mathcal{E}), tol, max\_ite$ 
Output:  $\Delta \mathbf{x}^1$ 
1 Find the warm start point  $\Delta \mathbf{x}^0$  by solving (19);
2 Find the intersection subspace  $\mathcal{U}_1^0$  by Algorithm 1;
  /* iteration until convergence. */
3 while  $step < max\_ite$  do
4   Find  $\Delta \mathbf{x}^1$  by solving (20);
5   Find the intersection subspace  $\mathcal{U}_1^1$  by Algorithm 1;
6   if  $\|\mathcal{U}_1^1 - \mathcal{U}_1^0\|_2 \leq tol$  then
7     break; /* converged. */
8   else
9      $\mathcal{U}_1^0 := \mathcal{U}_1^1$ ;
10  end
11 end

```

---

### D. Discussions on Full AC Model Design

In the previous sections, we theoretically established the robust MTD algorithm based on the simplified AC model (5)-(7) and intend to apply the algorithms on the full AC model (1)-(2). There exists similar concept on the weakest point in the original AC settings. Let  $\mathbf{h}'^{-1}(\cdot)$  represent the result of state estimation in (2). The estimated state on attacked measurement is written as  $\hat{\mathbf{v}}'_a = \mathbf{h}'^{-1}(\mathbf{z}'_a)$  and the residual is  $\gamma'_a = \|\mathbf{R}^{-\frac{1}{2}}(\mathbf{z}'_a - \mathbf{h}'(\hat{\mathbf{v}}'_a))\|_2^2$ . The weakest point can be defined as a unitary attack vector such that  $\gamma'_a$  is minimized. However, there are several obstacles to analytically write its expression. Firstly, recall that  $\mathbf{a} = \mathbf{h}(\mathbf{v}' + \mathbf{c}) - \mathbf{h}(\mathbf{v}')$  which is non-linearly dependent on post-MTD state  $\mathbf{v}'$  and state attack vector  $\mathbf{c}$ . Note that  $\mathbf{v}'$  is dependent on  $\mathbf{x}'$  which cannot be determined in advance. Second,  $\mathbf{h}'^{-1}(\cdot)$  requires iterative update, such as Gauss-Newton or Quasi-Newton algorithm. Although it is possible to reformulate AC-SE as semi-definite programming [38], it lacks of analytical solution in general. Third, it is difficult to define the concept of angles between subspaces defined by two functions  $\mathbf{h}(\cdot)$  and  $\mathbf{h}'(\cdot)$ . Consequently, we theoretically derived the robust algorithm based on the simplified AC model and numerically verify the performance on AC-FDI attacks in simulation. We found out that the MTD designed by the sufficient separation between the subspaces between the Jacobian matrices can provide effective detection in the full AC model.

## V. SIMULATION

### A. Simulation Set-ups

We test the proposed algorithms<sup>2</sup> on IEEE benchmarks case-6ww, case-14, and case-57 in MATPOWER [39]. AC-OPF is solved using python package PYPOWER 5.1.15. and the nonlinear optimization problems are solved using open-source library SciPy. More simulation set-ups are given as follows.

1) *Attack Pools and BDD Threshold*: Firstly, we define the attack strength with respect to the noise level as:

$$\rho = \frac{\|\mathbf{a}\|_2}{\sqrt{\sum_i^m \sigma_i^2}} \quad (21)$$

<sup>2</sup>Code is available at [https://github.com/xuwkk/Robust\\_MTD](https://github.com/xuwkk/Robust_MTD)

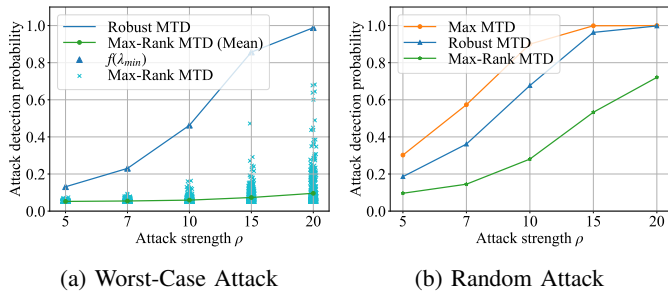


Figure 4: ADPs on simplified case-6 system.

We consider three types of attacks for the simplified AC model. 1). **Worst-case attack** where the attacker attacks on the weakest point  $u_{k+1}$  of a given MTD strategy according to Algorithm 1; 2). **Single-state attack** where the attacker only injects on single non-reference phase angle of the grid; and 3). **Random attack** where the attack vector  $\mathbf{a}$  is randomly generated as follows. Firstly, the attack state vector  $\mathbf{c}$  is generated with a random number of attacked states  $\|\mathbf{c}\|_0 = q, q = 1, 2, \dots, n$  and then sampled from multivariate Gaussian distribution with  $q$  non-zero entries. Then the attack vector is found as  $\mathbf{a} = \mathbf{J}\mathbf{c}$  and rescaled by different  $\rho = 5, 7, 10, 15, 20$  according to (21). To simplify the analysis, the measurement noise is set as  $\sigma_i = 0.01 p.u., \forall i$  in all the case studies. In this case, to have  $\beta$ -MTD, a necessary condition is  $\rho \geq \sqrt{\lambda_c(\beta)/m}$  according to Proposition 2.

The measurement in the original AC model consists of  $P_i, Q_i, P_{k:i \rightarrow j},$  and  $Q_{k:i \rightarrow j}$  (1). To simulate the attack with different attack strength, we randomly sample  $\mathbf{c}$  from uniform distribution and classify  $\mathbf{a} = \mathbf{h}'(\boldsymbol{\nu}' + \mathbf{c}) - \mathbf{h}'(\boldsymbol{\nu}')$  into one of the ranges  $\{[5, 7), [7, 10), [10, 15), [15, 20), [20, 25), [25, \infty)\}$  by (21).

We sample `no_load=50` load conditions on a uniform distribution of the default load profile in MATPOWER [39] for each grid. We then set the D-FACTS devices by robust MTD algorithms and simulate the real-time measurements. Under each load condition, we generate `no_attack=200` attack attempts for each of the attack types. The BDD threshold  $\tau_\chi(\alpha)$  is determined to have  $\alpha = 5\%$  FPR according different DoFs in different systems.

2) *Metrics and Baselines*: The key metric to evaluate the MTD detection performance is the true positive rate, also known as the attack detection probability (ADP) which is the ratio between the number of attacks that are detected by the MTD detector and the total number of attacks.

The max-rank MTD algorithm modified from [17]–[20] is compared as the baseline where the reactances are randomly changed with  $\mu_{min}\mathbf{x}_i \leq |\Delta\mathbf{x}_i| \leq \mu_{max}\mathbf{x}_i$ . Note that each reactance is perturbed by  $\mu_{min} > 0$  to fulfill max-rank condition on the composite matrix. For each one of the `no_attack` attack attempt, we simulate `no_maxrank=20` number of max rank MTDs to evaluate its average detection performance.

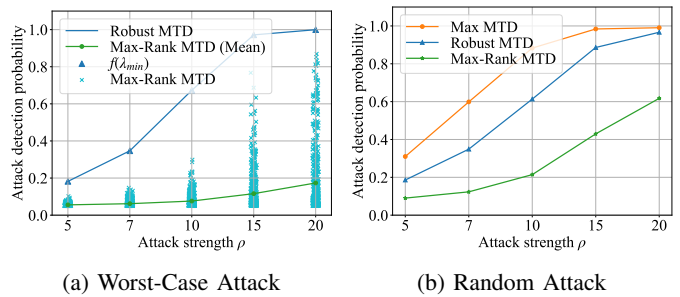


Figure 5: ADPs on simplified case-14 system.

## B. Verification of Theoretical Analysis on Simplified AC Model

In the first case study, we verify the theoretical analysis of robust MTD algorithms and demonstrate its effectiveness on the simplified AC model (5)-(7).

Firstly, the ADPs on case-6 with complete configuration are illustrated in Fig. 4 for both worst-case attacks and random attacks. The reactances are changed with  $\tau = 0.2$ . Meanwhile,  $\mu_{min} = 0.05$  and  $\mu_{max} = 0.2$  in the max-rank MTD. In Fig. 4(a), the simulation result on the ADPs of robust MTD is the same as the theoretic detection rate  $f(\lambda_{min})$  calculated by Proposition 3, which verifies the theoretic analysis and the design criteria. In addition, the robust MTD algorithm shows much higher ADPs than the max-rank MTD on the worst-case attack. Although the max-rank MTD's performance may approach to the robust MTD in some cases, its average ADP is similar to the FPR as the worst-case performance cannot be explicitly considered under the noiseless setting.

In Fig. 4(b), the max MTD is added by solving (9) with the assumption that the attack vector  $\mathbf{a}_N$  is known, which represents the performance upper-bound of any MTD design. As shown by Fig. 4(b), the robust MTD algorithm, not only guarantees the worst case condition, but also outperforms the max-rank MTD by 10%-45% on random attacks with different  $\rho$ . Moreover, the gap between robust MTD and max MTD algorithms is smaller than 25% and approaches to zero when  $\rho \geq 15$ . However, by comparing Fig. 4(a) and Fig. 4(b), it is worth noting that the major improvement of robust MTD over max-rank MTD still lays in the worst-case attacks.

Fig. 5 investigates the performance on the case-14 system with incomplete configuration. By Algorithm 1, the minimum  $k$  equals to 6 and the worst point in  $\mathcal{J}_N \setminus (\mathcal{J}'_N \cap \mathcal{J}_N)$  is at  $u_7$ . Assume that all branches are equipped with D-FACTS devices and the maximum perturbation ratio is set as  $\tau = 0.2$ . Although the detection rates on attacks in  $\mathcal{U}_1$  equal to  $\alpha$  according to Lemma 1, the ADP on  $u_7$  is nonzero by implementing Algorithm 2 and increases as the attack strength increases. Similar to Fig. 4(a), although the max-rank MTD algorithm can, by chance, give high detection rate against the worst case attack, its average detection rate is extremely low. In Fig. 5(b), the gap between max MTD and robust MTD is low (5%-30%). The results demonstrate that the robust design can also effectively improve the detection performance for the grid with incomplete configuration.

To further investigate on the weakest points in  $\mathcal{U}_1$ , we generate single-bus attack with  $\rho = 10$  and record the ADPs



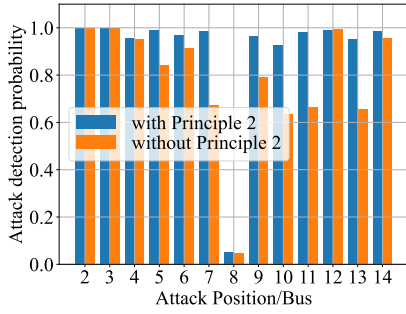


Figure 6: ADPs on single-state attacks of case-14 system.

in Fig. 6 with and without Principle 2 (17). Firstly, attacks targeting on bus-8 can only be detected by 5%. This is because bus-8 is a degree-one bus which is excluded by any loop. Second, with Principle 2 considered, the robust MTD can give more than 90% ADPs for all buses. In contrast, there are attacks against certain buses, e.g. bus-7, 10, 11, and 13 can be barely detected without Principle 2. Consequently, the simulation result verifies that Principle 2 can sufficiently reduce the chance of attacking on the weakest points.

### C. Simulation Results on Full AC Model

In this section, we verify the detection effectiveness of the proposed robust MTD algorithms on FDI attacks under the original AC settings (1)-(2).

1) *Random Attack*: The ADPs on random attacks for case-6, case-14, and case-57 systems are summarised in Table I. Similar to the studies on simplified AC models, the proposed robust algorithms can improve the ADPs by 10%-40% than the max-rank algorithm. In particular, for the cases with attack strength below 20, robust MTD can almost double the ADPs of max-rank MTD for all three systems. Therefore, the robust MTD designed by the principal angles between the subspaces of pre- and post- MTD Jacobian matrices can significantly improve the detection effectiveness for defending AC-FDI attacks. In addition, the attacks with larger attack strength are more likely to be detected while the detection probability for different systems under the same attack strength is slightly different due to their different load levels, parameters (e.g. the reactance to resistance ratios), and topologies. For instance, case-57 system is harder to detect as the ADPs in both max-rank and robust MTDs are lower than the case-6 and case-14 systems.

To certify the detection performance, the residual distributions for case-6, case-14, and case-57 systems are summarized in Fig. 7 where kernel density estimation (KDE) is used to smooth the histograms. The result implies that the proposed algorithms can generalize well on the AC-FDI attacks by sufficiently shifting the distribution positively, which is shown to be a key property on effective MTD with the measurement noise considered in Fig. 2. For each sub-figure, it can be observed that the detection probability without MTD is around 5% which is the same as the predefined FPR and on average, the max-rank MTD performs worse than the robust MTD.

Table I: Average ADPs on Random AC-FDI Attacks.

$\rho$	case-6		case-14		case-57	
	Max-Rk	Robust	Max-Rk	Robust	Max-Rk	Robust
$[5, 7)$	7.1%	13.7%	8.6%	18.1%	10.3%	30.3%
$[7, 10)$	12.6%	33.2%	14.4%	41.2%	15.2%	39.2%
$[10, 15)$	25.1%	67.3%	27.5%	63.1%	23.7%	55.9%
$[15, 20)$	44.5%	92.4%	43.4%	87.5%	36.0%	69.1%
$[20, 25)$	60.2%	98.2%	60.6%	94.5%	50.6%	81.6%

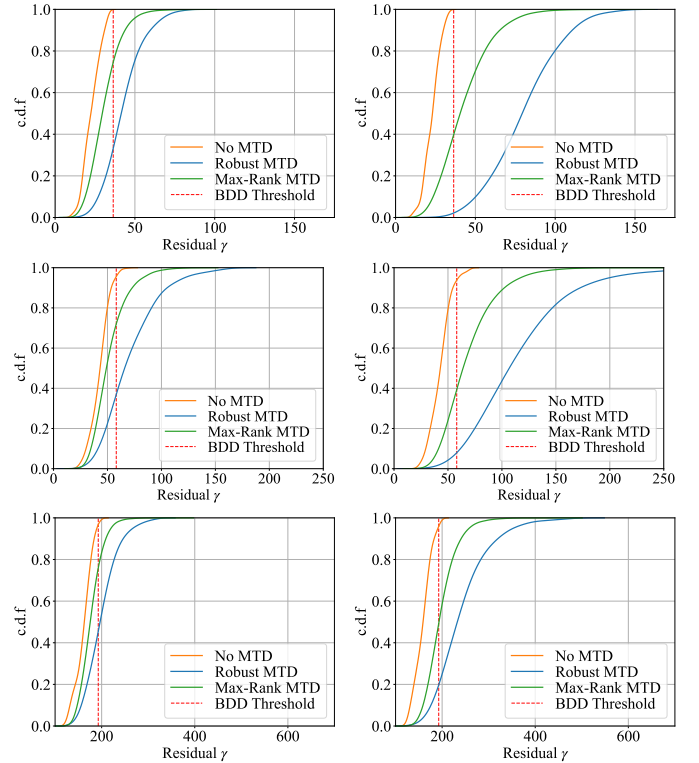


Figure 7: Residual distributions of AC FDI attacks. The first row: case-6 system; the second row: case-14 system; the third row: case-57 system; the first column: attacks in range  $[10, 15)$ ; the second column: attacks in range  $[20, 25)$ .

2) *Impact of Different Placements and Perturbation Ratios of D-FACTS Devices*: Fig. 8 records the simulation results on AC random attacks under two D-FACTS devices placements and four perturbation ratio limits. In detail, ‘all’ represents perturbing all branches whereas ‘part’ represents perturbing on branch- 2, 3, 4, 12, 15, 18, and 20, which is the outcome of the ‘D-FACTS Devices Placement Algorithm’ in Appendix E. Simulation result shows that  $k = 6$  is achieved and all buses are covered except bus 8 in ‘part’ placement. As the maximum perturbation ratio is reported as 50% in literature [21],  $\tau$  is set as 0.2, 0.3, 0.4, and 0.5. As a result, the grey curve in Fig. 8 is simulated under the same settings as the robust MTD in Table I. When the number of D-FACTS devices is limited, although the minimum  $k$  is still fulfilled by Principle 1, the detection rate is significantly reduced. In order to attain higher detection rate, the perturbation limit should be further increased. Notably, these findings on the dependency of ADP on different D-FACTS device placements and perturbation ratios can only be found when the sensor noise is considered.

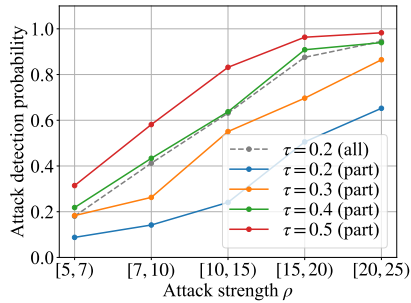


Figure 8: ADPs under different D-FACTS devices parameters.

3) *Computational Time*: The computational time of the proposed algorithms are summarized in Table II. While the computation time depends on the system scales, number of D-FACTS devices, and algorithms, they are acceptable for real-time applications. In practice, as the attackers spend time to learn the new parameters, the system operator can solve the robust MTD algorithms with period much larger than the state estimation time, e.g. several hours, or only change Jacobian matrix  $\mathbf{J}_N$  when the loads are significantly changed. A flat state vector may also be a choice to construct the Jacobian matrix if the loads change slowly. Multi-run strategy is also applied to approach to the global optimum of the nonlinear optimization problem.

Table II: Computational Time (averaged by no\_load runs).

Case	No. D-FACTS	Algorithm	Time (s)
case-6	11	(16)	0.022
	20	Algorithm 2	1.925
case-14	20	Algorithm 2 without (17)	0.325
	7	Algorithm 2	0.532
case-57	78	Algorithm 2	9.357

## VI. CONCLUSIONS

In this paper, we address the real-time robust implementation of MTD against unknown FDI attacks. Using the concept of angles between subspaces, we theoretically prove that the weakest point for any given MTD strategy corresponds to the smallest principal angle and the worst-case detection rate is proportional to the sine of this angle, with the impact of measurement noises being explicitly considered. These novel findings can help evaluate the effectiveness of the MTD strategy to tackle the unseen attacks in CPPS. A robust MTD algorithm is proposed by increasing the worst-case detection rate for the grid with complete MTD configuration. We then demonstrate that the weakest point(s) in incomplete MTD always exist and cannot be improved. Therefore, robust MTD for the grid with incomplete configuration is proposed by refraining from the ineffective MTD operation and improving the worst-case detection rate in the detectable subspace. Simulation results on standard IEEE benchmarks verify the real-time detection effectiveness on AC-FDI attacks, compared with the baseline.

## APPENDIX

### A. Proof of Proposition 1

The composite matrix of original and perturbed Jacobian matrix (6) is written as:

$$(\mathbf{J} \quad \mathbf{J}') = \mathbf{V} \begin{pmatrix} \mathbf{B} & -\mathbf{G} & \mathbf{B}' & -\mathbf{G}' \end{pmatrix} \begin{pmatrix} \mathbf{A}_r^{\cos} & \mathbf{0} \\ \mathbf{A}_r^{\sin} & \mathbf{0} \\ \mathbf{0} & \mathbf{A}_r^{\cos} \\ \mathbf{0} & \mathbf{A}_r^{\sin} \end{pmatrix}$$

Given the property of matrix product, the rank of the composite matrix satisfies that  $\text{rank}((\mathbf{J} \quad \mathbf{J}')) \leq \min\{m, m, 2n\}$ . If  $m < 2n$ ,  $\text{rank}((\mathbf{J} \quad \mathbf{J}')) \leq m < 2n$  no matter how the D-FACTS devices are altered. Therefore, the MTD cannot be complete if  $m < 2n$ .

### B. Normalized Measurement Vectors and Matrices

We consider measurement noise follows independent Gaussian distribution which is not necessarily isotropic. Let  $\mathbf{z}_N = \mathbf{R}^{-\frac{1}{2}}\mathbf{z}$ ,  $\mathbf{e}_N = \mathbf{R}^{-\frac{1}{2}}\mathbf{e}$ , and  $\mathbf{J}_N = \mathbf{R}^{-\frac{1}{2}}\mathbf{H}$ . The measurement equation becomes  $\mathbf{z}_N = \mathbf{J}_N\boldsymbol{\theta} + \mathbf{e}_N$ .  $\mathbf{P}_J$  which is defined on  $\langle \cdot, \cdot \rangle_{\mathbf{R}^{-\frac{1}{2}}}$ , now becomes  $\mathbf{P}_{J_N} = \mathbf{J}_N(\mathbf{J}_N^T\mathbf{J}_N)^{-1}\mathbf{J}_N^T$ , defined on  $\langle \cdot, \cdot \rangle$ . Similarly,  $\mathbf{S}_{J_N} = \mathbf{I} - \mathbf{P}_{J_N}$ . It is easy to show that  $\mathbf{R}^{-\frac{1}{2}}\mathbf{S}_J = \mathbf{S}_{J_N}\mathbf{R}^{-\frac{1}{2}}$ . As a result,  $\mathbf{r}(\mathbf{z}_N) = \mathbf{S}_{J_N}\mathbf{e}_N$  follows (approximately) standard normal distribution  $\mathbf{r}(\mathbf{z}_N) \sim \mathcal{N}(\mathbf{0}, \mathbf{I})$ . In the paper, we write  $\mathbf{P}_{J_N}$  and  $\mathbf{S}_{J_N}$  as  $\mathbf{P}_N$  and  $\mathbf{S}_N$  in short.

### C. Proof of Proposition 2

Firstly, a  $\beta$ -MTD is to have  $\|\mathbf{S}'_N\mathbf{a}_N\|_2 \geq \sqrt{\lambda_c(\beta)}$ . The necessary condition then follows from  $\|\mathbf{S}'_N\mathbf{a}_N\|_2 \leq \|\mathbf{S}_N\|_2\|\mathbf{a}_N\|_2 = \|\mathbf{a}_N\|_2$ .

Moreover, as  $\mathbf{a}_N = \mathbf{R}^{-\frac{1}{2}}\mathbf{a}$ , it also gives  $\|\mathbf{S}'_N\|_2\|\mathbf{R}^{-\frac{1}{2}}\|\|\mathbf{a}\|_2 = \|\mathbf{R}^{-\frac{1}{2}}\|\|\mathbf{a}\|_2 \geq \sqrt{\lambda_c(\beta)}$ . As  $\|\mathbf{R}^{-\frac{1}{2}}\| = \max\sigma(\mathbf{R}^{-\frac{1}{2}}) = \sigma_{\min}^{-1}$ , it can be derived that  $\|\mathbf{a}\|_2 \geq \sigma_{\min}\sqrt{\lambda_c(\beta)}$ . Furthermore, if  $\mathbf{R} = \text{diag}([\sigma, \sigma, \dots, \sigma])$  is isotropic, then it gives  $\|\mathbf{R}^{-\frac{1}{2}}\mathbf{a}\|_2 = \sigma^{-1}\|\mathbf{a}\|_2 \geq \sqrt{\lambda_c(\beta)}$ . Let  $\rho = \|\mathbf{a}\|_2/\sqrt{\sum_i^m\sigma_i^2}$ . It also gives  $\rho \geq \sqrt{\lambda_c(\beta)}/\sqrt{m}$ .

### D. Proof of Proposition 3

According to Definition 1, the weakest point  $\mathbf{j}_N^* \in \mathcal{J}_N$ ,  $\|\mathbf{j}_N^*\|_2 = 1$  can be derived by

$$\begin{aligned} \mathbf{j}_N^* &= \arg \min_{\substack{\mathbf{j}_N \in \mathcal{J}_N \\ \|\mathbf{j}_N\|_2=1}} \sqrt{\lambda_{eff}} \\ &= \arg \min_{\substack{\mathbf{j}_N \in \mathcal{J}_N \\ \|\mathbf{j}_N\|_2=1}} \frac{\|\mathbf{j}_N - \mathbf{P}'_N\mathbf{j}_N\|_2}{\|\mathbf{j}_N\|_2} \\ &= \arg \min_{\substack{\mathbf{j}_N \in \mathcal{J}_N \\ \|\mathbf{j}_N\|_2=1}} \sin \angle \{\mathbf{j}_N, \mathbf{P}'_N\mathbf{j}_N\} \end{aligned} \quad (\text{A.1})$$

Note that the triangle relationship within sides  $\|\mathbf{j}_N\|$ ,  $\|\mathbf{P}'_N\mathbf{j}_N\|$ , and  $\|\mathbf{j}_N - \mathbf{P}'_N\mathbf{j}_N\|$  and the ratio in (A.1) is the sine of the angle between vectors  $\mathbf{j}_N$  and  $\mathbf{P}'_N\mathbf{j}_N$ . Basing on the definition of principal angle (11), the sine of the angle is minimized when  $\angle\{\mathbf{j}_N, \mathbf{P}'_N\mathbf{j}_N\} = \theta_1$ . The minimum principal angle is achieved when  $\mathbf{j}_N$  and  $\mathbf{P}'_N\mathbf{j}_N$  are reciprocal such that  $\mathbf{j}_N = \mathbf{u}_1$  and  $\mathbf{P}'_N\mathbf{j}_N = \mathbf{P}'_N\mathbf{u}_1 = \cos\theta_1\mathbf{v}_1$  [34], [40].

Moreover, the worst-case detection rate is achieved when attacking on  $\mathbf{u}_1$  such that

$$\lambda_{min} = \|\mathbf{a}\mathbf{u}_1 - a \cos \theta_1 \mathbf{v}_1\|_2^2 = a^2 \sin^2 \theta_1$$

### E. D-FACTS Devices Placement

A modified minimum edge covering algorithm is proposed to find the smallest number of D-FACTS devices covering all buses while satisfying the minimum  $k$  condition. The pseudo code is given by Algorithm 3. In detail, the inputs to the proposed MTD deployment algorithm are the grid information  $\mathcal{G}(\mathcal{N}, \mathcal{E})$  and the output is branch set  $\mathcal{E}_D$ . In line 1-2, CB represents the function to calculate the set of cycle basis of a given graph. Algorithm 3 then removes any buses that is not included by cycle basis (thus not in any loops) and the corresponding branches from grid  $\mathcal{G}$ . In line 3-4, the minimum edge covering (MEC) problem is solved. Given the power grid topology, MEC firstly runs the maximum (cardinality) matching algorithm to find the maximum branch set whose ending buses are not incident to each other [36]. The maximum matching is found by Edmonds' BLOSSOM algorithm where the size of the initial empty matching is increased iteratively along the so-called augmenting path spotted by blossom contraction [36]. After constructing the maximum matching, a greedy algorithm is carried out to add any uncovered buses to the maximum matching set. The resulting branch set becomes  $\mathcal{E}_D$ , the minimum edge covering set where each bus is connected with at least one branch. Line 5-16 guarantees the minimum- $k$  requirement where it breaks edge in any identified cycle bases in  $\bar{\mathcal{G}}_2$ . At last, line 11-13 is added to avoid adding any new loop in  $\bar{\mathcal{G}}_1$ .

---

#### Algorithm 3: D-FACTS Devices Placement Algorithm

---

```

Input :  $\mathcal{G}(\mathcal{N}, \mathcal{E})$ 
Output:  $\mathcal{E}_D$ 
1  $\mathcal{L} = \text{CB}(\mathcal{G})$ ; /* find the circle basis */
2 Find buses  $\mathcal{N}_1$  not in  $\mathcal{L}$ . Remove  $\mathcal{N}_1$  and the incident branches
   from  $\mathcal{G}$ . Name the resulting graph as  $\bar{\mathcal{G}}(\bar{\mathcal{N}}, \bar{\mathcal{E}})$ ;
3  $\mathcal{E}_{min} = \text{MEC}(\bar{\mathcal{G}})$ , construct  $\bar{\mathcal{G}}_1(\bar{\mathcal{N}}, \mathcal{E}_{min})$  and  $\bar{\mathcal{G}}_2(\bar{\mathcal{N}}, \mathcal{E}_r)$  with
    $\mathcal{E}_r = \bar{\mathcal{E}} \setminus \mathcal{E}_{min}$ ;
4  $\mathcal{L}_2 = \text{CB}(\bar{\mathcal{G}}_2)$  /* loops in non D-FACTS graph */
5 for loop in  $\mathcal{L}_2$  do
6   for  $e$  in loop do
7     Construct  $\bar{\mathcal{G}}_1(\bar{\mathcal{N}}, \mathcal{E}_{min})$  and  $\bar{\mathcal{G}}_2(\bar{\mathcal{N}}, \mathcal{E}_r)$  where
        $\mathcal{E}_{min} \leftarrow \mathcal{E}_{min} + e$  and  $\mathcal{E}_r \leftarrow \mathcal{E}_r - e$ ;
8      $\mathcal{L}_1 = \text{CB}(\bar{\mathcal{G}}_1)$ ;
       /* loops in D-FACTS graph */
9     if  $\mathcal{L}_1 = \emptyset$  then
10      break
11    else
12       $\bar{\mathcal{G}}_1(\bar{\mathcal{N}}, \mathcal{E}_{min})$  and  $\bar{\mathcal{G}}_2(\bar{\mathcal{N}}, \mathcal{E}_r)$  where
         $\mathcal{E}_{min} \leftarrow \mathcal{E}_{min} - e$  and  $\mathcal{E}_r \leftarrow \mathcal{E}_r + e$ ;
13    end
14  end
15 end

```

---

### F. Proof of Lemma 1

Rewrite the non-centrality parameter as

$$\begin{aligned} \sqrt{\lambda} &= \|(\mathbf{I} - \mathbf{V}\mathbf{V}^T)\mathbf{U}\mathbf{c}\|_2 \\ &= \|(\mathbf{U} - \mathbf{V}\Sigma)\mathbf{c}\|_2 \\ &= \|((\mathbf{U}_1, \mathbf{U}_{23}) - (\mathbf{V}_1\Sigma_1, \mathbf{V}_{23}\Sigma_{23}))\mathbf{c}\|_2 \end{aligned} \quad (\text{A.2})$$

As  $\mathbf{U}_1 = \mathbf{V}_1$  and  $\Sigma_1 = \mathbf{I}$ , (A.2) can be reduced into  $\sqrt{\lambda} = \|(\mathbf{U}_{23} - \mathbf{V}_{23}\Sigma_{23})\mathbf{c}_{23}\|_2$  which does not depend on  $\mathbf{c}_1$ .

### REFERENCES

- [1] C.-W. Ten, C.-C. Liu, and G. Manimaran, "Vulnerability assessment of cybersecurity for scada systems," *IEEE Transactions on Power Systems*, vol. 23, no. 4, pp. 1836–1846, 2008.
- [2] A. S. Musleh, G. Chen, and Z. Y. Dong, "A survey on the detection algorithms for false data injection attacks in smart grids," *IEEE Transactions on Smart Grid*, vol. 11, no. 3, pp. 2218–2234, 2019.
- [3] Y. Liu, P. Ning, and M. K. Reiter, "False data injection attacks against state estimation in electric power grids," *ACM Transactions on Information and System Security (TISSEC)*, vol. 14, no. 1, pp. 1–33, 2011.
- [4] G. Hug and J. A. Giampapa, "Vulnerability assessment of ac state estimation with respect to false data injection cyber-attacks," *IEEE Transactions on Smart Grid*, vol. 3, no. 3, pp. 1362–1370, 2012.
- [5] M. A. Rahman and H. Mohsenian-Rad, "False data injection attacks against nonlinear state estimation in smart power grids," in *2013 IEEE Power & Energy Society General Meeting*. IEEE, 2013, pp. 1–5.
- [6] S. Ahmed, Y. Lee, S.-H. Hyun, and I. Koo, "Unsupervised machine learning-based detection of covert data integrity assault in smart grid networks utilizing isolation forest," *IEEE Transactions on Information Forensics and Security*, vol. 14, no. 10, pp. 2765–2777, 2019.
- [7] A. Gómez-Expósito, A. J. Conejo, and C. Cañizares, *Electric energy systems: analysis and operation*. CRC press, 2018.
- [8] A. Tajer, "False data injection attacks in electricity markets by limited adversaries: Stochastic robustness," *IEEE Transactions on Smart Grid*, vol. 10, no. 1, pp. 128–138, 2017.
- [9] L. Xie, Y. Mo, and B. Sinopoli, "Integrity data attacks in power market operations," *IEEE Transactions on Smart Grid*, vol. 2, no. 4, pp. 659–666, 2011.
- [10] J. Kim, L. Tong, and R. J. Thomas, "Subspace methods for data attack on state estimation: A data driven approach," *IEEE Transactions on Signal Processing*, vol. 63, no. 5, pp. 1102–1114, 2014.
- [11] Z.-H. Yu and W.-L. Chin, "Blind false data injection attack using pca approximation method in smart grid," *IEEE Transactions on Smart Grid*, vol. 6, no. 3, pp. 1219–1226, 2015.
- [12] S. Lakshminarayana, A. Kammoun, M. Debbah, and H. V. Poor, "Data-driven false data injection attacks against power grids: A random matrix approach," *IEEE Transactions on Smart Grid*, vol. 12, no. 1, pp. 635–646, 2021.
- [13] J.-H. Cho, D. P. Sharma, H. Alavizadeh, S. Yoon, N. Ben-Asher, T. J. Moore, D. S. Kim, H. Lim, and F. F. Nelson, "Toward proactive, adaptive defense: A survey on moving target defense," *IEEE Communications Surveys & Tutorials*, vol. 22, no. 1, pp. 709–745, 2020.
- [14] K. L. Morrow, E. Heine, K. M. Rogers, R. B. Bobba, and T. J. Overbye, "Topology perturbation for detecting malicious data injection," in *2012 45th Hawaii International Conference on System Sciences*, 2012, pp. 2104–2113.
- [15] K. R. Davis, K. L. Morrow, R. Bobba, and E. Heine, "Power flow cyber attacks and perturbation-based defense," in *2012 IEEE Third International Conference on Smart Grid Communications (SmartGridComm)*, 2012, pp. 342–347.
- [16] M. A. Rahman, E. Al-Shaer, and R. B. Bobba, "Moving target defense for hardening the security of the power system state estimation," in *Proceedings of the First ACM Workshop on Moving Target Defense*, 2014, pp. 59–68.
- [17] C. Liu, J. Wu, C. Long, and D. Kundur, "Reactance perturbation for detecting and identifying fdi attacks in power system state estimation," *IEEE Journal of Selected Topics in Signal Processing*, vol. 12, no. 4, pp. 763–776, 2018.
- [18] Z. Zhang, R. Deng, D. K. Yau, P. Cheng, and J. Chen, "Analysis of moving target defense against false data injection attacks on power grid," *IEEE Transactions on Information Forensics and Security*, vol. 15, pp. 2320–2335, 2019.
- [19] B. Liu and H. Wu, "Optimal d-facts placement in moving target defense against false data injection attacks," *IEEE Transactions on Smart Grid*, vol. 11, no. 5, pp. 4345–4357, 2020.
- [20] Z. Zhang, R. Deng, P. Cheng, and M.-Y. Chow, "Strategic protection against fdi attacks with moving target defense in power grids," *IEEE Transactions on Control of Network Systems*, pp. 1–1, 2021.
- [21] S. Lakshminarayana and D. K. Yau, "Cost-benefit analysis of moving-target defense in power grids," *IEEE Transactions on Power Systems*, vol. 36, no. 2, pp. 1152–1163, 2021.

- [22] C. Liu, H. Liang, T. Chen, J. Wu, and C. Long, "Joint admittance perturbation and meter protection for mitigating stealthy fdi attacks against power system state estimation," *IEEE Transactions on Power Systems*, vol. 35, no. 2, pp. 1468–1478, 2019.
- [23] J. Tian, R. Tan, X. Guan, Z. Xu, and T. Liu, "Moving target defense approach to detecting stuxnet-like attacks," *IEEE transactions on smart grid*, vol. 11, no. 1, pp. 291–300, 2019.
- [24] M. Higgins, F. Teng, and T. Parisini, "Stealthy mtd against unsupervised learning-based blind fdi attacks in power systems," *IEEE Transactions on Information Forensics and Security*, vol. 16, pp. 1275–1287, 2020.
- [25] B. Li, G. Xiao, R. Lu, R. Deng, and H. Bao, "On feasibility and limitations of detecting false data injection attacks on power grid state estimation using d-facts devices," *IEEE Transactions on Industrial Informatics*, vol. 16, no. 2, pp. 854–864, 2019.
- [26] A. Abur and A. G. Exposito, *Power system state estimation: theory and implementation*. CRC press, 2004.
- [27] J. Zhang, Y. Wang, Y. Weng, and N. Zhang, "Topology identification and line parameter estimation for non-pmu distribution network: A numerical method," *IEEE Transactions on Smart Grid*, vol. 11, no. 5, pp. 4440–4453, 2020.
- [28] J. Zhao, G. Zhang, M. La Scala, Z. Y. Dong, C. Chen, and J. Wang, "Short-term state forecasting-aided method for detection of smart grid general false data injection attacks," *IEEE Transactions on Smart Grid*, vol. 8, no. 4, pp. 1580–1590, 2017.
- [29] W. Xu and F. Teng, "A deep learning based detection method for combined integrity-availability cyber attacks in power system," *arXiv preprint arXiv:2011.01816*, 2020.
- [30] C. Liu, R. Deng, W. He, H. Liang, and W. Du, "Optimal coding schemes for detecting false data injection attacks in power system state estimation," *IEEE Transactions on Smart Grid*, 2021.
- [31] K. Krishnamoorthy, *Handbook of statistical distributions with applications*. Chapman and Hall/CRC, 2006.
- [32] A. Teixeira, S. Amin, H. Sandberg, K. H. Johansson, and S. S. Sastry, "Cyber security analysis of state estimators in electric power systems," in *49th IEEE conference on decision and control (CDC)*. IEEE, 2010, pp. 5991–5998.
- [33] C. D. Meyer, *Matrix analysis and applied linear algebra*. Siam, 2000, vol. 71.
- [34] A. Galántai, "Subspaces, angles and pairs of orthogonal projections," *Linear and Multilinear Algebra*, vol. 56, no. 3, pp. 227–260, 2008.
- [35] Z. Galil, "Efficient algorithms for finding maximum matching in graphs," *ACM Computing Surveys (CSUR)*, vol. 18, no. 1, pp. 23–38, 1986.
- [36] J. A. Bondy and U. S. R. Murty, *Graph theory*. Springer, 2008, vol. 244.
- [37] Z. Zhang, R. Deng, D. K. Yau, P. Cheng, and J. Chen, "On hiddenness of moving target defense against false data injection attacks on power grid," *ACM Transactions on Cyber-Physical Systems*, vol. 4, no. 3, pp. 1–29, 2020.
- [38] H. Zhu and G. B. Giannakis, "Power system nonlinear state estimation using distributed semidefinite programming," *IEEE Journal of Selected Topics in Signal Processing*, vol. 8, no. 6, pp. 1039–1050, 2014.
- [39] R. D. Zimmerman, C. E. Murillo-Sánchez, and R. J. Thomas, "Matpower: Steady-state operations, planning, and analysis tools for power systems research and education," *IEEE Transactions on Power Systems*, vol. 26, no. 1, pp. 12–19, 2011.
- [40] A. Ben-Israel and T. N. Greville, *Generalized inverses: theory and applications*. Springer Science & Business Media, 2003, vol. 15.